crystals

MDPI

Article

Efficiency Properties of Cerium-Doped Lanthanum Chloride ($LaCl_3$:Ce) Single Crystal Scintillator under Radiographic X-ray Excitation

Stavros Tseremoglou [1], Christos Michail [1], Ioannis Valais [1], Konstantinos Ninos [2], Athanasios Bakas [2], Ioannis Kandarakis [1], George Fountos [1] and Nektarios Kalyvas [1,*]

[1] Radiation Physics, Materials Technology and Biomedical Imaging Laboratory, Department of Biomedical Engineering, University of West Attica, Ag. Spyridonos, 12210 Athens, Greece; stseremoglou@uniwa.gr (S.T.); cmichail@uniwa.gr (C.M.); valais@uniwa.gr (I.V.); kandarakis@uniwa.gr (I.K.); gfoun@uniwa.gr (G.F.)

[2] Department of Biomedical Sciences, University of West Attica, Ag. Spyridonos, 12210 Athens, Greece; kninos@uniwa.gr (K.N.); abakas@uniwa.gr (A.B.)

* Correspondence: nkalyvas@uniwa.gr; Tel.: +30-21053-85319

Abstract: The aim of this study is to evaluate the suitability of crystalline scintillator $LaCl_3$:Ce for possible use in hybrid medical imaging systems, such as PET/CT and SPECT/CT scanners. For this purpose, a single crystal ($10 \times 10 \times 10$ mm^3) was irradiated by X-rays within the tube voltage range from 50 to 150 kVp, and the absolute efficiency (AE) was measured experimentally. The energy absorption efficiency (EAE), quantum detection efficiency (QDE), and the spectral compatibility with various optical detectors were also calculated with the use of mathematical formulas. The results were compared with published data for $Bi_4Ge_3O_{12}$ (BGO), Lu_2SiO_5:Ce (LSO), and $CdWO_4$ single crystals of equal dimensions, commonly used in medical imaging applications. The luminescence efficiency values of the examined crystal were found to be higher than those of LSO, BGO, and $CdWO_4$ crystals, within the whole X-ray tube voltage range. In the matter of EAE, $LaCl_3$:Ce demonstrated reduced performance with respect to LSO and $CdWO_4$ crystals. The emission spectrum of $LaCl_3$:Ce was found to be compatible with various types of photocathodes and silicon photomultipliers (SiPMs). Considering these properties, $LaCl_3$:Ce crystal could be considered suitable for use in hybrid medical imaging systems.

Keywords: scintillators; single crystals; radiation detectors; $LaCl_3$:Ce

Citation: Tseremoglou, S.; Michail, C.; Valais, I.; Ninos, K.; Bakas, A.; Kandarakis, I.; Fountos, G.; Kalyvas, N. Efficiency Properties of Cerium-Doped Lanthanum Chloride ($LaCl_3$:Ce) Single Crystal Scintillator under Radiographic X-ray Excitation. *Crystals* **2022**, *12*, 655. https://doi.org/10.3390/cryst12050655

Academic Editor: Jesús Sanmartín-Matalobos

Received: 14 March 2022
Accepted: 1 May 2022
Published: 4 May 2022

1. Introduction

Scintillators are materials particularly important in medical imaging systems, because their use may reduce the ionizing radiation dose to the patient. Scintillation detectors are usually connected to optical sensors, such as film, photocathodes, photodiodes, CCD, a-Si/TFT, and CMOS [1–4]. The latter setup has been widely employed in several technological fields, from industry up to nuclear physics, but with a prominent application in medical imaging applications such as X-ray imaging, computed tomography (CT), single photon emission computed tomography (SPECT), and positron emission tomography (PET) [4–8]. The sensitivity, which is antagonistic to patient dose, of these systems increases remarkably when more efficient and faster scintillation crystals are utilized [5,8].

Crystal scintillator's investigation is of major importance in nuclear medicine systems. As an example, crystalline scintillators with halogenated impurities, such as lanthanum chloride ($LaCl_3$) activated with cerium (Ce), has been widely studied in nuclear medicine applications [9–11] because of its physical properties, such as a density of 3.86 g/cm^3 suitable for radiation absorption, a high light output reported from 40.000 photons/MeV to 49.000 photons/MeV), a decay time of 28 ns, and good energy resolution, which depends upon the crystal physical and chemical properties such as size and cerium concentration [10,12–18].

The $LaCl_3$:Ce crystal has an hexagonal symmetry in the UCl_3 type lattice in the space group $P6_3/m$ or C^2_{6h}, with point symmetry C_{3h} at the lanthanide site. The lanthanide coordination polyhedron consists of nine chloride ligands arranged in a tricapped trigonal prism configuration [15,19]. The lattice constant of the crystal is 0.6196 nm [13]. The con-centration of cerium in the crystal has been reported in the literature to be from 0.1% to 30% [11,12,15,20].

Current nuclear medicine instrumentation includes hybrid systems where contemporary imaging systems such as SPECT and PET are combined with X-ray computed tomography scanners (CT) and form hybrid systems such as SPECT/CT and PET/CT. A breakthrough of such a hybrid modality could be the use of the same detector type for CT and SPECT or PET.

Under this consideration, in the current work, the response of a commercially available $LaCl_3$:Ce single crystal scintillator [13] excitation was experimentally examined for X-ray tube voltages in the range from 50 kVp to 150 kVp. The response was examined via (a) the absolute luminescence efficiency (*AE*), describing the light output power per incident exposure, (b) the spectral matching factor (α_s) and the overall efficiency (*EE*), investigating the suitability of various photodetectors attached to $LaCl_3$:Ce, and (c) the radiation absorption properties of the crystal. After research into the relevant literature, excitation of $LaCl_3$:Ce crystal with X-rays to investigate some of its properties was carried out in specific energy ranges. The crystal's emission spectrum, after X-ray excitation produced by X-ray tube at 35 kV with 25 mA, has been studied by Guillot-Noel et al. [15]. This study was supplemented by the usage of $LaCl_3$:Ce crystals of different concentrations of cerium, under the same experimental conditions [12]. The emission spectrum of the crystal was also measured at 30 kV with 25 mA [20]. In order to investigate the crystal suitability, mainly for X-ray counting applications, studies of the proportionality of response and the energy resolution of the crystal have also been carried out in the energy ranges 10.5–100 keV [21] and 5–60 keV (X-rays from radioactive sources Fe-55: 5.9 keV, Cd-109: 22 keV, and Am-241: 60 keV) [22]. This work extends the current $LaCl_3$:Ce literature and presents a combined examination of $LaCl_3$:Ce performance in terms of measuring absolute efficiency in clinical utilized X-ray tube voltages, calculating the X-ray energy absorption efficiency and estimating the suitability of $LaCl_3$:Ce in conjunction with commercially available photoreceptors, with the scope of using $LaCl_3$:Ce in hybrid medical imaging systems.

The results of this study were compared with calculated and previously published results for $Bi_4Ge_3O_{12}$ (BGO), Lu_2SiO_5:Ce (LSO), and $CdWO_4$ single crystals that are commonly used in several imaging systems [23,24], and the specific $LaCl_3$:Ce crystal absolute efficiency was found comparable or better.

High light yield (i.e., *AE*) as well as satisfactory spectral matching to optical sensors (α_s and EE) yields scintillator–photodetector combinations which can provide higher signal output and better image quality for a given level of patient exposure. Accordingly, a required quality of output image can be obtained with less radiation burden to the examinee. The latter is important in CT examinations where a lot of X-ray projections are obtained per gantry rotation and scan.

2. Materials and Methods

A single cubic-shaped crystal was purchased from Advatech UK Limited [13]. The cube dimensions were $10 \times 10 \times 10$ mm^3. The light yield (*LY*) of the crystal was 49.000 photons/MeV (provided by the supplier), its density 3.86 g/cm^3, and its max emission peak is at 350 nm [13]. The surfaces of the crystal were polished. In addition, the crystal was purchased encapsulated in a thin aluminum protective layer, due to its hygroscopicity, where only one crystal surface, i.e., output, was not encapsulated. Energy absorption efficiency (*EAE*), quantum detection efficiency (*QDE*), absolute luminescence efficiency (AE), spectral matching factors (SMF), and effective efficiency (*EE*) with several optical detectors were determined experimentally or with the use of mathematical formulas. The X-ray flux needed for absolute efficiency calculation was obtained by an X-ray tube coupled with a

CPI, series CMP 200DR 50 kW generator. The high voltage ranged from 50 to 150 kVp and the current–time product was kept constant at 63 mA s. The inherent filtration of the X-ray tube was 1.5 mm Al. Furthermore, an additional Al filtration of 20 mm was placed at the tube exit [7,23–25].

The quantum detection efficiency (*QDE*) describes the ability of a scintillator to detect photons and is defined as the fraction of the incident X-rays interacting with the scintillator [26]. The fraction of the incident X-ray energy absorbed in the crystal is described through the energy absorption efficiency (*EAE*) [26]. EAE and QDE can be calculated as [23,26]:

$$EAE(E) = \frac{\int_0^{E_0} \Phi_0\,(E) E \left(\frac{\mu_{en}\,(E)/\rho}{\mu_{att}(E)/\rho}\right)\left(1 - e^{-(\mu_{att}\,(E)/\rho)\rho T}\right) dE}{\int_0^{E_0} \Phi_0\,(E) E dE} \quad (1)$$

and

$$QDE = \frac{\int_0^{E_0} \Phi_0\,(E)\left(1 - e^{-(\mu_{att}\,(E)/\rho)\rho T}\right) dE}{\int_0^{E_0} \Phi_0\,(E) dE} \quad (2)$$

where $\Phi_0(E)$ is the incident X-ray photon fluence on the scintillator, E is the photon energy, $\mu_{att}(E)/\rho$ is the radiation photon total mass attenuation coefficient, and $\mu_{en}(E)/\rho$ is the corresponding total mass energy absorption coefficient. T is the detector thickness and ρ is the density (in g/cm^3) [23,26]. The coefficients used in Equations (1) and (2) were obtained from XMudat software [27], and the X-ray fluence from TASMIP Spectra Calculator [28].

The absolute luminescence efficiency is defined as the ratio of the energy flux $\dot{\Psi}_\lambda$ (units μW·m^{-2}) of the optical photons emitted by a stimulated crystal to the rate of exposure $\dot{X}$ (units mR·s^{-1}) of the X-rays incident on it [29]. The instrumentation necessary for measuring the optical photon flux comprised an Oriel light integration sphere, an EMI photomultiplier tube, and a Cary electrometer. More details regarding the measurement of *AE* can be obtained in the literature [7,23–25]. According to its definition [24,25],

$$AE = \dot{\Psi}_\lambda / \dot{X} \quad (3)$$

The units of *AE* are known as efficiency units (EU), where 1 EU = 1 μW·m^{-2}/(mR·s^{-1}).

Crystal scintillators are always combined with optical photon detectors. The performance of such a combination can be estimated by the spectral matching factor α_s, which expresses the spectral compatibility of the scintillator's emitted light to the spectral sensitivity of the photodetector, and it can be defined as [23]

$$\alpha_s = \frac{\int S_p(\lambda) S_D(\lambda) d\lambda}{\int S_p(\lambda) d\lambda} \quad (4)$$

where $S_p(\lambda)$ is the spectrum of the emitted light by the scintillator, $S_D(\lambda)$ is the spectral sensitivity of the photodetector coupled to the scintillator, and λ is the wavelength of the light emitted [30]. The spectral sensitivity of various photodetectors was obtained from manufacturers' data and the literature [25,31–34].

The overall efficiency of a scintillator–photodetector combination has been expressed by the effective efficiency (*EE*) [35] and is calculated as [8,25]

$$EE = AE \cdot \alpha_s \quad (5)$$

3. Results and Discussion

Figure 1 shows values for the energy absorption efficiency of the $LaCl_3$:Ce crystal. These values were compared with calculated data for BGO, LSO, and $CdWO_4$ single crystals of equal dimensions. The *EAE* values of $LaCl_3$:Ce crystal were lower than BGO, LSO, and $CdWO_4$ in the low-energy range (50 kVp) (0.497 for $LaCl_3$:Ce, 0.840 for BGO, 0.871 for LSO, and 0.714 for $CdWO_4$) as a consequence of the significantly higher density of these

materials (7.13, 7.4, and 7.9 g/cm^3, respectively) [23,36,37] in regard to the 3.86 g/cm^3 of $LaCl_3$:Ce. The deviation between the absorption efficiency values of $LaCl_3$:Ce and those of BGO, LSO, and $CdWO_4$ decreases as the X-ray energy increases. At 70 kVp, $LaCl_3$:Ce shows a tendency to increase, but remains lower than the EAE of LSO and $CdWO_4$ crystals. At 150 kVp, the *EAE* values of $LaCl_3$:Ce, BGO, LSO, and $CdWO_4$ are approximately 0.584, 0.698, 0.566, and 0.587, respectively. The highest values for $LaCl_3$:Ce were calculated at 140 and 150 kVp, demonstrating that the use of $LaCl_3$:Ce of this thickness favors higher energy radiographic applications such as computed tomography.

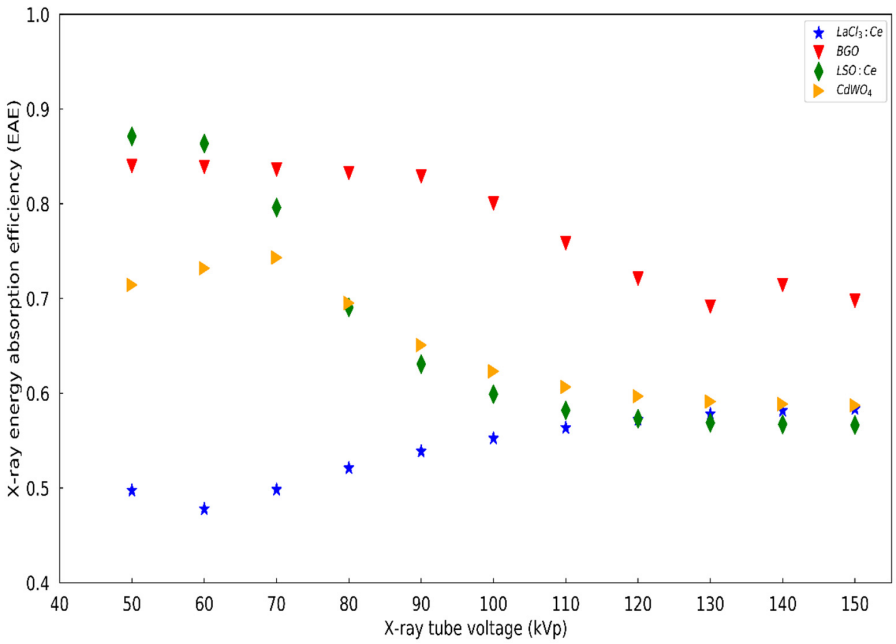

Figure 1. EAE of the $LaCl_3$:Ce, BGO, LSO:Ce, and $CdWO_4$ single crystals.

The attenuation coefficients, as well as the ratio of the attenuation coefficients μ_{en}/μ_{att} used in Equations (1) and (2), are shown in Figures 2 and 3, respectively, for all four materials.

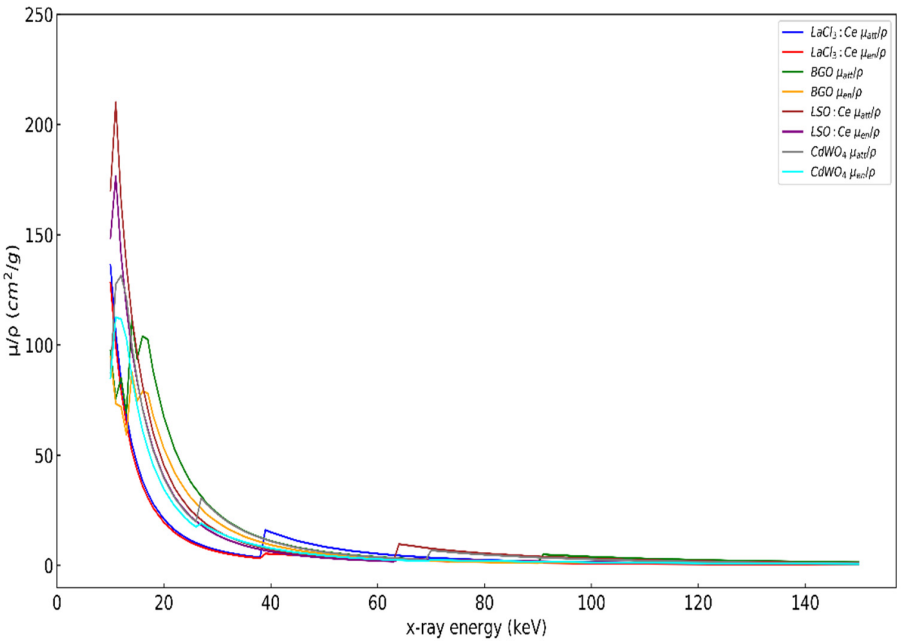

Figure 2. Attenuation coefficients of the $LaCl_3$:Ce, BGO, LSO, and $CdWO_4$ single crystals.

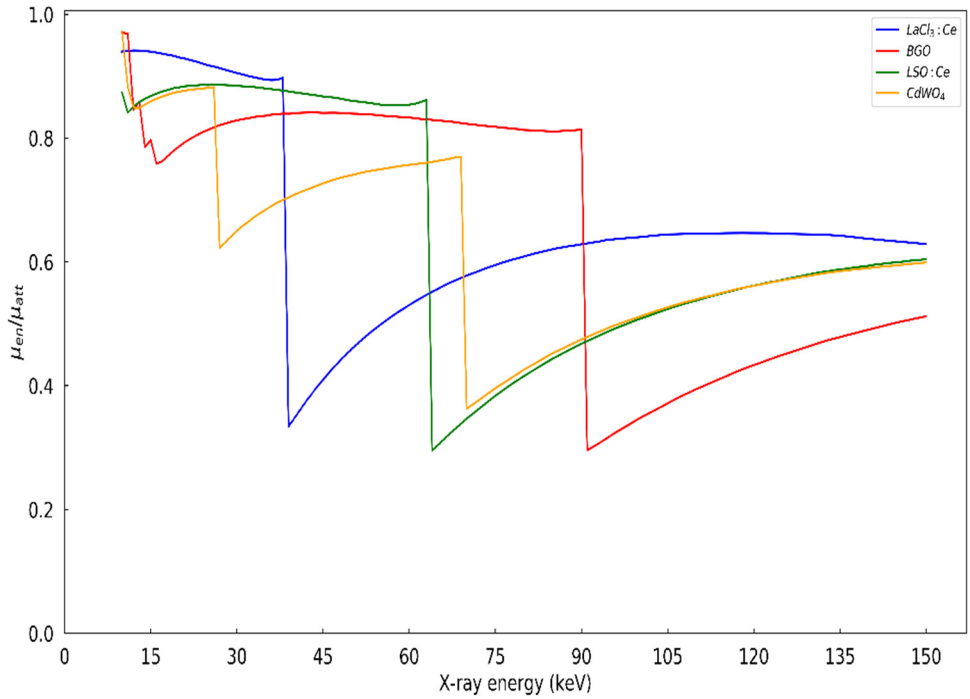

Figure 3. Attenuation coefficients ratio μ_{en}/μ_{att} of the $LaCl_3$:Ce, BGO, LSO, and $CdWO_4$ single crystals.

As shown in Figure 1, the *EAE* generally decreases when increasing the voltage across the X-ray tube. The ability of a crystal to absorb photons is expressed through the attenuation coefficient μ_{att} and the absorption coefficient μ_{en}. μ_{att} expresses the probability of interaction of the radiation with the crystal, which is manifested mainly through photoelectric effect, based on the energies and the effective atomic number (Z_{eff}) of these crystals. μ_{en} expresses the probability of absorbing radiation inside the crystal. With increasing voltage in the X-ray tube, the emitted radiation spectrum moves to higher energies. As the energies of the emitted photons increase, the μ_{att} coefficients decrease, as shown in Figure 2, except for some energy values at which some discontinuities occur. These discontinuities are called absorption edges and correspond to binding energies of the K, L, M, and N shells, where the probability of photon absorption through the photoelectric effect is greatly increased due to resonance. In addition, as shown in Figure 3, the ratio μ_{en}/μ_{att} at some energy values decreases sharply, and, as a consequence, the *EAE* of the crystal decreases. This reduction for BGO and LSO:Ce crystals occurs at the K-edges energy values. Specifically, for BGO, this reduction occurs at 90 keV, therefore the *EAE* of the crystal decreases after 90 kVp with a tendency to stabilize after 120 kVp, due to the observed small recovery of the corresponding curve in Figure 3. For LSO:Ce and $CdWO_4$ crystals, this reduction occurs at 63 KeV and 69 keV, respectively, and, consequently, the *EAE* of these crystals decreases after 63 kVp and 69 kVp, respectively, while stabilizing after 110 kVp for both crystals at about the same levels as shown in Figure 3. For $LaCl_3$:Ce crystal, the reduction is at 38 keV and the effect in the corresponding curve in Figure 1, although not clearly visible, explains the reduction of EAE from 50 kVp to 60 kVp. The increase of *EAE* after 60 kVp and its stabilization after 110 kVp, at the same levels as the LSO:Ce and $CdWO_4$ crystals, is explained by the high increase of the μ_{en}/μ_{att} ratio of the crystal after 38 keV and its tendency to equate with the values of the μ_{en}/μ_{att} ratio of the other two crystals.

Figure 4 illustrates the fluctuation of *QDE* values with X-ray tube voltage. It is apparent from these values that $LaCl_3$:Ce of thickness 10 mm exhibits almost perfect efficiency to detect the incident photos, as the values range from 0.996 to 1.

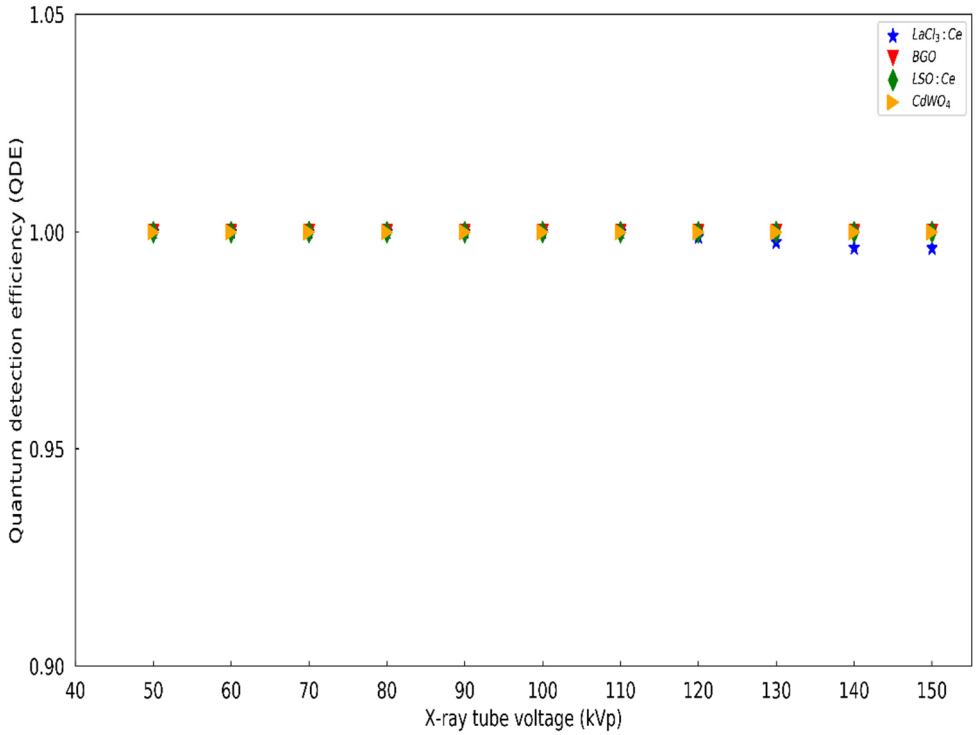

Figure 4. Quantum detection efficiency of the $LaCl_3$:Ce single crystal in comparison with BGO, LSO, and $CdWO_4$ single crystals.

The variation of the purchased $LaCl_3$:Ce absolute efficiency with X-ray tube voltages 50 to 150 kVp is shown in Figure 5. In Figure 5, the corresponding AE values for LSO, BGO, and $CdWO_4$ crystals of equal dimensions ($10 \times 10 \times 10$ mm^3) are also demonstrated [23,24]. The *AE* values of all crystals demonstrate a tendency to increase with increasing of the kVp. However, $LaCl_3$:Ce values were in all cases higher than those of the other crystals. For example, at the tube voltages applied of 70 kVp and 130 kVp, the absolute efficiencies were (a) for 70 kVp: 24.38 EU for $LaCl_3$:Ce, 18.7 EU for $CdWO_4$, 12.4 *EU* for LSO, and 2.3 *EU* for BGO; and (b) for 130 kVp: 38.7 *EU* for $LaCl_3$:Ce, 26.9 *EU* for $CdWO_4$, 17.7 *EU* for LSO, and 3.7 *EU* for BGO [23,24]. The *AE* results confirm the suitability of $LaCl_3$:Ce crystal for possible use in medical imaging applications, since it exhibits higher values than LSO and BGO single crystals, which are commonly used in such applications. Furthermore, the AE values in higher energies verify the efficiency of $LaCl_3$:Ce crystal in nuclear medicine applications.

It is worth commenting that the increased efficiency of $LaCl_3$:Ce, compared to $CdWO_4$, LSO, and BGO, cannot be attributed only to its radiation absorption properties. A reason that can explain its increased absolute efficiency is the additional effect of its higher light yield (*LY*) 49.000 photons/MeV compared to the 8.900 photons/MeV for BGO crystal, 30.000 photons/MeV for LSO crystal, and 28.000 photons/MeV for $CdWO_4$ scintillator. The total number of the optical photons produced per incident X-ray, *L*, are due to the combined effect of *EAE* and *LY*. In order to theoretically estimate the total number of optical photons produced for several X-ray tube voltages, we calculated the mean energy $\overline{E}$ for the X-ray spectra at 50 kV, 60 kV, 80 kV, 140 kV, and 150 kV as $\overline{E} = \int \Phi(E)EdE / \int \Phi(E)dE$. The corresponding mean energies were calculated as 41.5 keV, 47.2 keV, 56.7 keV, 74.8 keV, and 75.9 keV, respectively. The total number of optical photons produced was calculated as $EAE \cdot \left(\frac{\overline{E}}{1000}\right) \cdot LY$.

In Table 1, the L values of $LaCl_3$:Ce, compared to $CdWO_4$, LSO, and BGO, at 50 kV, 60 kV, 80 kV, 140 kV, and 150 kV are shown.

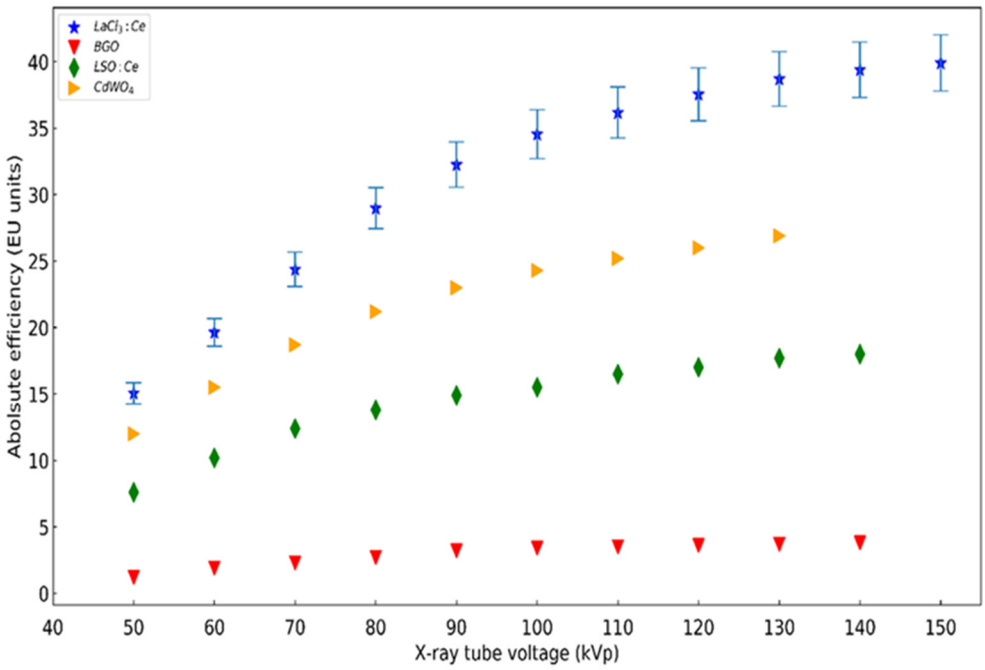

Figure 5. AE values of the $LaCl_3$:Ce single crystal in comparison with previously published data for BGO, LSO, and $CdWO_4$ single crystals. The error bars correspond to 5.3%.

Table 1. Theoretical calculation of the number of optical photons generated in the crystal scintillators.

kVp	$LaCl_3$:Ce	$CdWO_4$	LSO	BGO
50	1011	830	1085	310
60	1105	968	1223	352
80	1448	1104	1174	420
140	2132	1233	1273	475
150	2170	1248	1290	471

It may be seen that for low X-ray energies, $LaCl_3$:Ce is inferior to LSO in terms of optical photon production, because of the low EAE, due to its low density and despite its higher light yield compared to LSO. For higher energies though, where the EAE differences between $LaCl_3$:Ce and LSO are reduced, as shown in Figure 1, $LaCl_3$:Ce produces more optical photons. In each case, however, the *AE* values of $LaCl_3$:Ce are superior to the scintillators at the X-ray tube voltages under investigation. This indicates that the optical photon propagation properties, such as transmission through the material and optical escape from the crystal, also play an important role in the total scintillation efficiency. The BGO, LSO, and $CdWO_4$ crystals were wrapped with Teflon layers as part of the irradiation procedure [38]. According to the literature, the reflectivity of the surfaces of polished crystals alone, or in contact with Teflon or specular surfaces, is close to 100% for optical photon angle of incidence over 30 degrees [39].

Figures 6–9 illustrate the normalized optical spectrum of $LaCl_3$:Ce crystal along with the spectral sensitivities of various optical sensors [25,31–34]. The $LaCl_3$:Ce spectrum, obtained from the vendor's website [13], shows the main luminescence peak at 350 nm [13,14].

The spectral matching factor values for $LaCl_3$:Ce, along with several optical detectors, were calculated according to Equation (4). These optical detectors, which are shown in Figures 6–9, were silicon photomultipliers (SiPMs) utilized in nuclear medicine techniques, charge-coupled devices (CCD), and complementary metal–oxide semiconductors (CMOS) used in imaging applications, as well as various photocathodes. It was found that $LaCl_3$:Ce exhibits excellent compatibility with multialkali photocathode (0.99), GaAs photocathode (0.93), and bialkali photocathode (0.94). Moreover, it exhibits exceptional compatibility when coupled with various flat panel (FP) photocathodes, with the SMF values fluctuating

from 0.91 to 0.99 (0.99 for H8500D-03 and H10966A). On the other hand, poor compatibility was registered with the GaAsP phosphor photocathode, since the SMF value was only 0.27. $LaCl_3$:Ce also showed good compatibility with most of the silicon photomultipliers used in our experiments, as it showed SMF values in the range from 0.62 to 0.67 (0.67 for Si PM S10985-050C and Si PM S10362-11-025U). On the contrary, $LaCl_3$:Ce was found to be incompatible with CCDs and CMOS detectors. Specifically, the lowest SMF values were registered for CCD with polygates (0.002), for CMOS RadEye HR (0.0), for CMOS Pgate (0.0002), and for CCD with traditional polygates and CCD no polygates (both at 0.0003). The combinations with SMF greater than 0.60 are shown in Table 2.

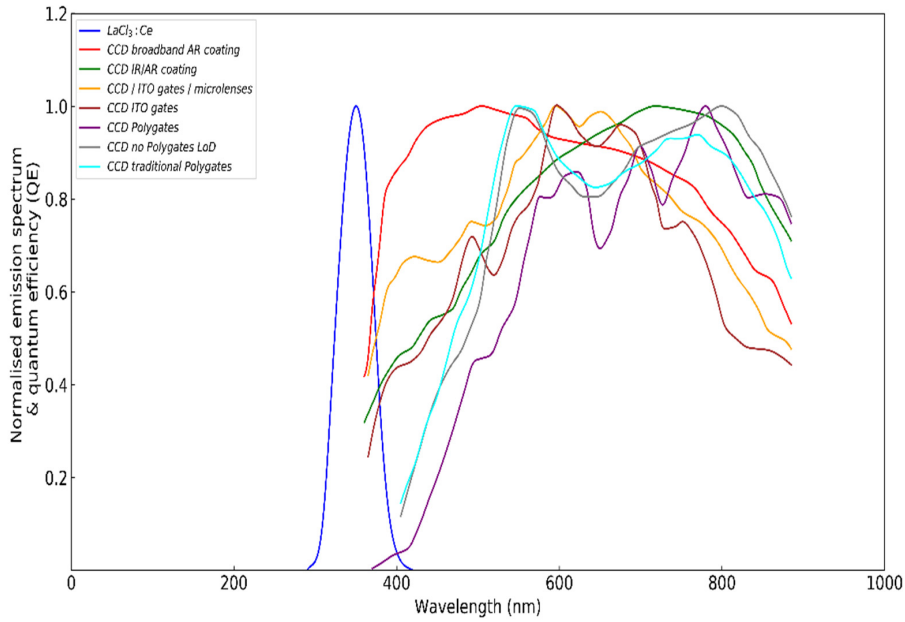

Figure 6. Normalized emitted light spectrum of the $LaCl_3$:Ce crystal and spectral sensitivity of various charge-coupled devices.

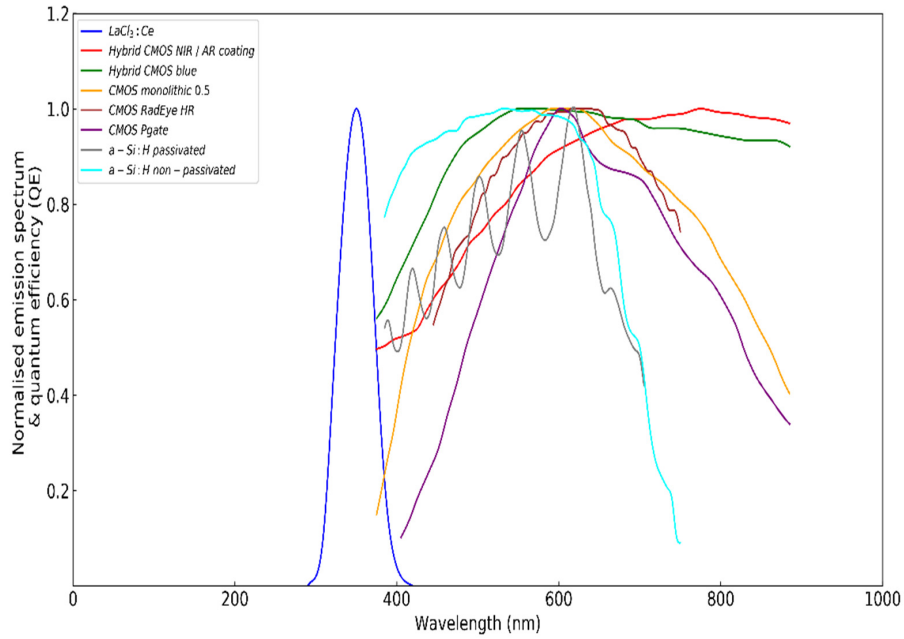

Figure 7. Normalized emitted light spectrum of the $LaCl_3$:Ce crystal and spectral sensitivity of various complementary metal–oxide semiconductors.

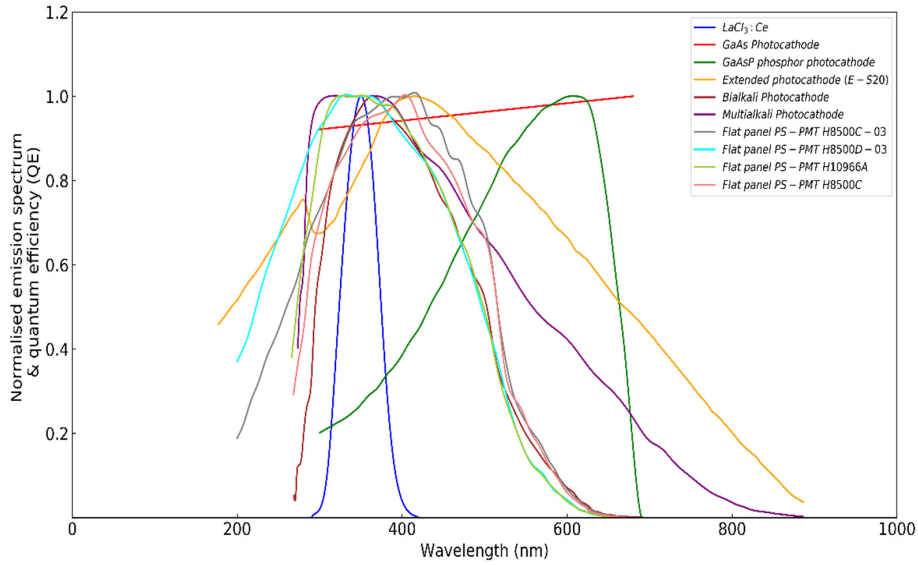

Figure 8. Normalized emitted light spectrum of the $LaCl_3$:Ce crystal and spectral sensitivity of various photocathodes.

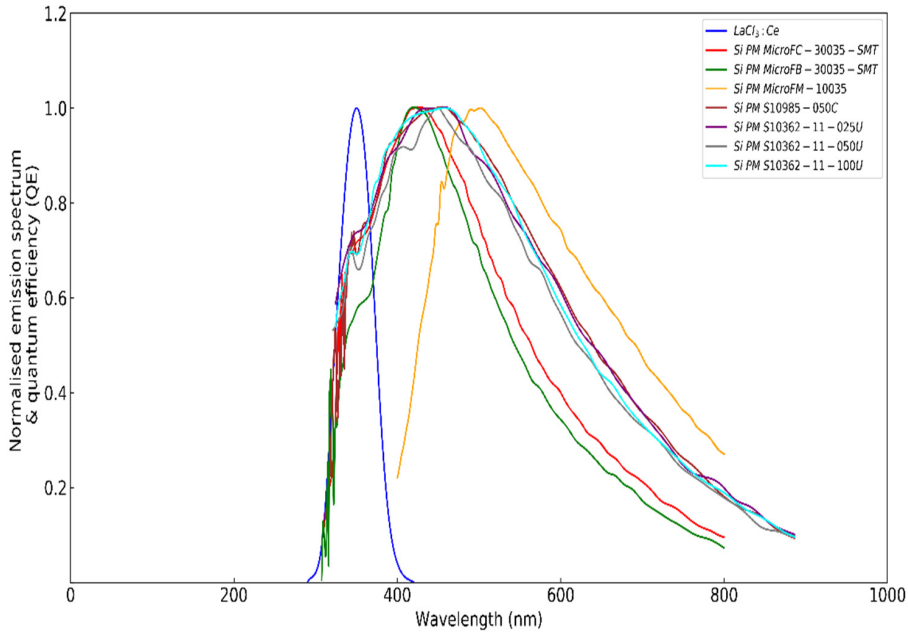

Figure 9. Normalized emitted light spectrum of the $LaCl_3$:Ce crystal and spectral sensitivity of various silicon photomultipliers.

Figures 10–13 illustrate the effective luminescence efficiency of the $LaCl_3$:Ce crystal with the optical detectors shown in Figures 6–9. The optimum effective efficiency values were attributed to photocathodes and silicon photomultipliers (SiPMs). The lowest values are obtained when coupled with CCDs and CMOS optical sensors. In detail, EE values almost equal to the AE ones are obtained (~15 EU at 50 kVp and ~39 EU at 150 kVp) when $LaCl_3$:Ce is coupled with GaAs photocathode, bialkali photocathode, multialkali photocathode, flat panel PS-PMT H8500D-03, and flat panel PS-PMT H10966A. On the contrary, the decrease (with kVp) in the detected luminescence signal varied from 99.7% to 100% when $LaCl_3$:Ce was combined with CMOS RadEye HR, CMOS Pgate, CCD with polygates, CCD no polygates LoD, and CCD with traditional polygates.

Table 2. $LaCl_3$:Ce photodetector combinations with SMF above 0.60.

Optical Detectors	$LaCl_3$:Ce
Extended photocathode (E-S20)	0.83
Bialkali Photocathode	0.94
Multialkali Photocathode	0.99
(FP) PS-PMT H8500C-03	0.93
(FP) PS-PMT H8500D-03	0.99
(FP) PS-PMT H10966A	0.99
(FP)PS-PMT H8500C	0.91
SiPM MicroFC-30035-SMT	0.66
SiPM S10985-050C	0.67
SiPM S10362-11-025U	0.67
SiPM S10362-11-050U	0.62
SiPM S10362-11-100U	0.65
GaAs Photocathode	0.93

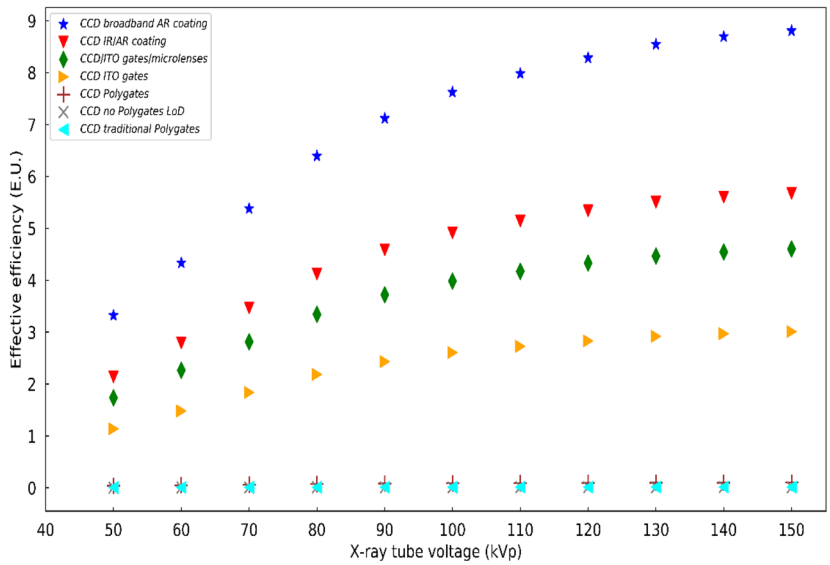

Figure 10. Effective efficiency of the $LaCl_3$:Ce crystal combined with various charge-coupled devices.

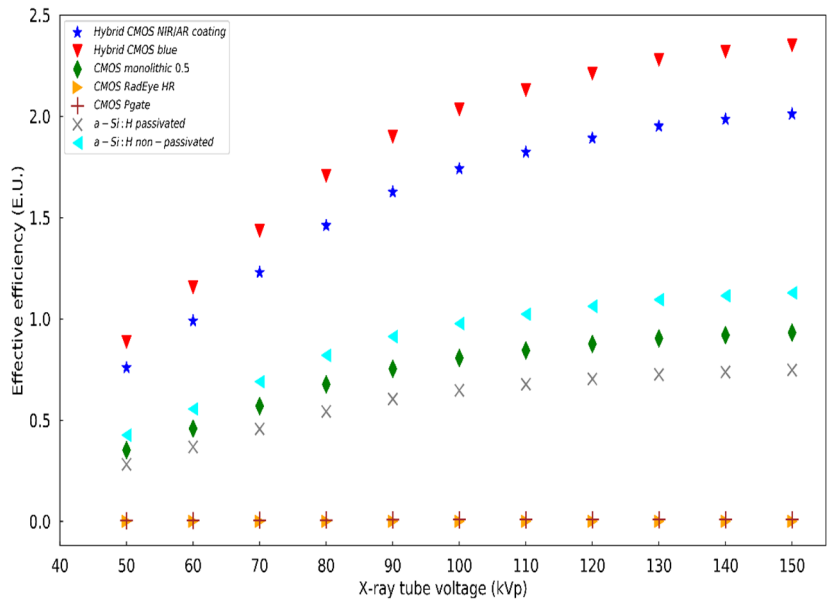

Figure 11. Effective efficiency of the $LaCl_3$:Ce crystal combined with various complementary metal–oxide semiconductors.

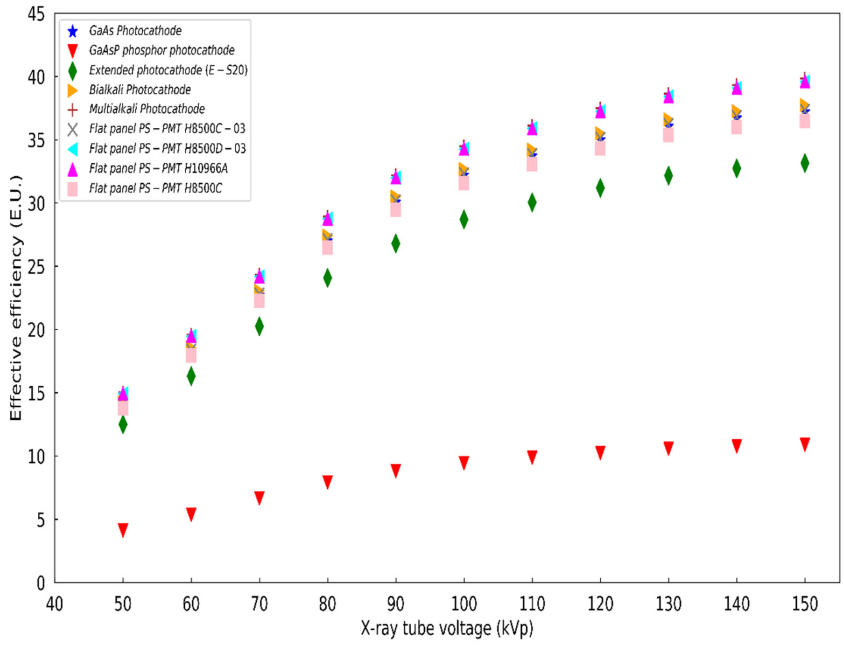

Figure 12. Effective efficiency of the $LaCl_3$:Ce crystal combined with various photocathodes.

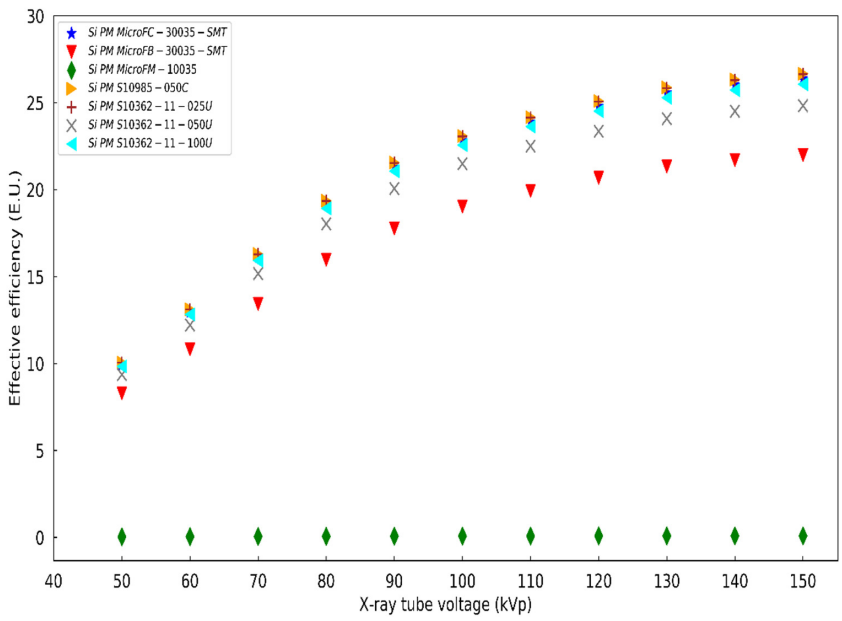

Figure 13. Effective efficiency of the LaCl3:Ce crystal combined with various silicon photomultipliers.

4. Conclusions

The absolute luminescence efficiency and the spectral matching of a $LaCl_3$:Ce crystal were examined within the tube voltage range (50–150 kVp) employed in X-ray imaging applications. The results were compared with previously published data for LSO, BGO, and $CdWO_4$ single crystals of equal dimensions, commonly utilized in commercial imaging systems. Peak absolute luminescence efficiency of $LaCl_3$:Ce crystal was obtained at 150 kVp (39.9 EU) The luminescence efficiency values of the examined crystal were found to be higher than those of LSO, BGO, and $CdWO_4$ crystals, within the whole X-ray tube voltage range. In terms of EAE, $LaCl_3$:Ce demonstrated reduced performance with respect to LSO and $CdWO_4$ crystals. The spectral compatibility with several commercial optical detectors was also investigated. The emission spectrum of $LaCl_3$:Ce was found to be compatible with various types of photocathodes and silicon photomultipliers (SiPMs).

A high-efficiency detector for hybrid medical imaging systems such as SPECT/CT and PET/CT would require reduced pharmaceutical administered activity for a given signal output. In addition, for the X-ray part of the system, reduced radiation translated to reduced current in the CT generator circuit, would be required. More specifically, if absolute efficiency measurements are considered, for the 140 kV X-ray irradiation conditions, $LaCl_3$:Ce can provide the same output as LSO and BGO with 46% and 10% of radiation exposure, respectively. Thus, a scintillator such as $LaCl_3$:Ce with optimized exposure conditions is expected to reduce patient exposure as well as the aforementioned operational costs of the medical installation.

Considering these properties and the previous studies examining $LaCl_3$:Ce crystal for use in nuclear medicine applications, $LaCl_3$:Ce crystal could be considered suitable for use in hybrid medical imaging systems, such as PET/CT and SPECT/CT scanners.

Author Contributions: Conceptualization, S.T., C.M. and N.K.; methodology, S.T., C.M., I.V., G.F. and N.K.; software, S.T. and I.V.; validation, K.N., G.F. and I.K.; formal analysis, S.T., C.M., I.V. and A.B.; investigation, S.T., I.K., A.B. and K.N.; resources, C.M., I.V. and G.F.; data curation, I.V. and N.K.; writing—original draft preparation, S.T., C.M. and N.K.; writing—review and editing, S.T., C.M., I.K. and N.K.; visualization, C.M. and N.K.; supervision, N.K.; project administration, C.M. and N.K. All authors have read and agreed to the published version of the manuscript.

Funding: This research received no external funding.

Conflicts of Interest: The authors declare no conflict of interest.

References

1. Mineev, O.V.; Kudenko, Y.G.; Musienko, Y.V.; Polyansky, I.; Yershov, N. Scintillator detectors with long WLS fibers and multi-pixel photodiodes. *J. Instrum.* **2011**, *6*, P12004. [CrossRef]
2. Vandenbroucke, A.; Foudray, A.M.; Olcott, P.D.; Levin, C.S. Performance characterization of a new high resolution PET scintillation detector. *Phys. Med. Biol.* **2010**, *55*, 5895–5911. [CrossRef] [PubMed]
3. Cha, B.K.; Kim, J.; Kim, Y.; Yun, S.; Cho, G.; Kim, H.; Seo, C.; Jeon, S.; Huh, Y. Design and image-quality performance of high resolution CMOS-based X-ray imaging detectors for digital mammography. *J. Instrum.* **2012**, *7*, C04020. [CrossRef]
4. Nassalski, A.; Kapusta, M.; Batsch, T.; Wolski, D.; Mockel, D.; Enghardt, W.; Moszynski, M. Comparative Study of Scintillators for PET/CT Detectors. *IEEE Trans. Nucl. Sci.* **2007**, *54*, 3–10. [CrossRef]
5. Nikl, M. Scintillation Detectors for X-rays. *Meas. Sci. Technol.* **2006**, *17*, R37. [CrossRef]
6. Valais, I.; Kandarakis, I.; Nikolopoulos, D.; Sianoudis, I.; Dimitropoulos, N.; Cavouras, D.; Nomicos, C.; Panayiotakis, G.S. Luminescence efficiency of Gd_2SiO_5:Ce scintillator under x-ray excitation. *IEEE Trans. Nucl. Sci.* **2005**, *52*, 1830–1835. [CrossRef]
7. Valais, I.; Kandarakis, I.; Nikolopoulos, D.; Michail, C.; David, S.; Loudos, G.; Cavouras, D.; Panayiotakis, G.S. Luminescence properties of $(Lu,Y)_2SiO_5$:Ce and Gd_2SiO_5:Ce single crystal scintillators under X-ray excitation for use in medical imaging systems. *IEEE Trans. Nucl. Sci.* **2007**, *54*, 11–18. [CrossRef]
8. Valais, I. Systematic Study of the Light Emission Efficiency and the Corresponding Intrinsic Physical Characteristics Of Single Crystal Scintillators, Doped with the Trivalent Cerium (Ce^{3+}) Activator, in Wide Energy Range (from 20 kV–18 MV) for Medical Applications. Ph.D. Thesis, University of Patras, Patras, Greece, 2008.
9. Alzimami, K.; Abuelhia, E.; Podolyak, Z.; Ioannou, A.; Spyrou, N.M. Characterization of $LaBr_3$:Ce and $LaCl_3$:Ce scintillators for gamma-ray spectroscopy. *J. Radioanal. Nucl. Chem.* **2008**, *278*, 755–759. [CrossRef]
10. Balcerzyk, M.; Moszynski, M.; Kapusta, M. Comparison of $LaCl_3$:Ce and NaI(Tl) scintillators in γ-ray spectrometry. *Nucl. Instrum. Methods Phys. Res. A* **2005**, *537*, 50–56. [CrossRef]
11. Shah, K.S.; Glodo, J.; Klugerman, M.; Cirignano, L.J.; Moses, W.; Derenzo, S.E.; Weber, M.J. $LaCl_3$:Ce scintillator for γ-ray detection. *Nucl. Instrum. Methods Phys. Res. Sect. A-Accel. Spectrometers Detect. Assoc. Equip.* **2003**, *505*, 76–81. [CrossRef]
12. Van Loef, E.V.D.; Dorenbos, P.; Van Eijk, C.W.E.; Kramer, K.; Gudel, H.U. Scintillation properties of $LaCl_3$:Ce^{3+} crystals: Fast, efficient and high-energy-resolution scintillators. In Proceedings of the 2000 IEEE Nuclear Science Symposium. Conference Record (Cat. No.00CH37149), Lyon, France, 15–20 October 2000; Volume 1, pp. 6/31–6/34. [CrossRef]
13. Advatech UK. LaCl3:Ce—Lanthanum Chloride (Ce). Available online: https://www.advatech-uk.co.uk/lacl3_ce.html (accessed on 25 June 2021).
14. Iltis, A.; Mayhugh, M.R.; Menge, P.; Rozsa, C.M.; Selles, O.; Solovyev, V. Lanthanum halide scintillators: Properties and applications. *Nucl. Instrum. Methods Phys. Res. Sect. A Accel. Spectrometers Detect. Assoc. Equip.* **2006**, *563*, 359–363. [CrossRef]
15. Guillot-Noel, O.; Haas, J.T.; Dorenbos, P.; Eijk, C.W.; Krämer, K.W.; Güdel, H.U. Optical and scintillation properties of cerium-doped $LaCl_3$, $LuBr_3$ and $LuCl_3$. *J. Lumin.* **1999**, *85*, 21–35. [CrossRef]

16. Moszynski, M.; Nassalski, A.; Syntfeld-Każuch, A.; Szczęśniak, T.; Czarnacki, W.; Wolski, D.; Pausch, G.; Stein, J. Temperature dependences of $LaBr_3$(Ce), $LaCl_3$(Ce) and NaI(Tl) scintillators. *Nucl. Instrum. Methods Phys. Res. Sect. A Accel. Spectrometers Detect. Assoc. Equip.* **2006**, *568*, 739–751. [CrossRef]
17. Van Eijk, C.W.E. Inorganic scintillators in medical imaging. *Phys. Med. Biol.* **2002**, *47*, R85–R106. [CrossRef] [PubMed]
18. Van Eijk, C.W.E. Inorganic-scintillator development. *Nucl. Instrum. Methods Phys. Res. Sect. A Accel. Spectrometers Detect. Assoc. Equip.* **2001**, *460*, 1–14. [CrossRef]
19. Antonyak, O.T.; Dorenbos, P.; Rodnyi, P.; Stryganyuk, G.B.; Voloshinovskii, A.S.; Zimmerer, G. *Luminescence Spectra of $LaCl_3$-Ce Crystals*; Hamburger HASYLAB at DESY: Hamburg, Germany, 2000.
20. Higgins, W.M.; Glodo, J.; Van Loef, E.V.D.; Klugerman, M.; Gupta, T.; Cirignano, L.; Wong, P.; Shah, K.S. Bridgman growth of $LaBr_3$:Ce and $LaCl_3$:Ce crystals for high-resolution gamma-ray spectrometers. *J. Cryst. Growth* **2006**, *287*, 239–242. [CrossRef]
21. Owens, A.; Bos, A.J.J.; Brandenburg, S.; Dorenbos, P.; Drozdowski, W.; Ostendorf, R.W.; Quarati, F.; Webb, A.; Welter, E. The hard X-ray response of Ce-doped lanthanum halide scintillators. *Nucl. Instrum. Methods Phys. Res. A* **2007**, *574*, 158–162. [CrossRef]
22. Martin, T.; Allier, C.; Bernard, F. Lanthanum Chloride Scintillator for X-ray Detection. *AIP Conf. Proc.* **2007**, *879*, 1156–1159. [CrossRef]
23. Michail, C.; Koukou, V.; Martini, N.; Saatsakis, G.; Kalyvas, N.; Bakas, A.; Kandarakis, I.; Fountos, G.; Panayiotakis, G.; Valais, I. Luminescence Efficiency of Cadmium Tungstate ($CdWO_4$) Single Crystal for Medical Imaging Applications. *Crystals* **2020**, *10*, 429. [CrossRef]
24. Michail, C.; Kalyvas, N.; Bakas, A.; Ninos, K.; Sianoudis, I.; Fountos, G.; Kandarakis, I.; Panayiotakis, G.; Valais, I. Absolute Luminescence Efficiency of Europium-Doped Calcium Fluoride (CaF_2:Eu) Single Crystals under X-ray Excitation. *Crystals* **2019**, *9*, 234. [CrossRef]
25. Linardatos, D.; Konstantinidis, A.; Valais, I.; Ninos, K.; Kalyvas, N.; Bakas, A.; Kandarakis, I.; Fountos, G.; Michail, C. On the Optical Response of Tellurium Activated Zinc Selenide ZnSe:Te Single Crystal. *Crystals* **2020**, *10*, 961. [CrossRef]
26. Boone, J. X-ray production, interaction, and detection in diagnostic imaging. In *Handbook of Medical Imaging. Volume 1: Physics and Psychophysics*; Beutel, J., Kundel, H.L., Van Metter, R.L., Eds.; SPIE Press: Bellingham, WA, USA, 2000; Volume 1, pp. 36–57. ISBN 978-0-8194-7772-9.
27. Nowotny, R. *XMuDat: Photon Attenuation Data on PC (IAEA-NDS-195)*; International Atomic Energy Agency: Vienna, Austria, 1998.
28. TASMIP Spectra Calculator. Available online: https://www.solutioinsilico.com/medical-physics/applications/tasmip-app.php?ans=0 (accessed on 14 March 2022).
29. Kandarakis, I.; Cavouras, D.; Panayiotakis, G.S.; Nomicos, C.D. Evaluating X-ray detectors for radiographic applications: A comparison of ZnSCdS:Ag with Gd_2O_2S:Tb and Y_2O_2S:Tb screens. *Phys. Med. Biol.* **1997**, *42*, 1351–1373. [CrossRef] [PubMed]
30. Kandarakis, I.; Cavouras, D.; Nomicos, C.D.; Panayiotakis, G.S. X-ray luminescence of ZnSCdS:Au, Cu phosphor using X-ray beams for medical applications. *Nucl. Instr. Meth. Phys. Res. B* **2001**, *179*, 215–224. [CrossRef]
31. Hamamatsu Photonics, MPPC (Multi-Pixel Photon Counters). Available online: http://www.hamamatsu.com/us/en/product/category/3100/4004/4113/index.html# (accessed on 3 July 2021).
32. Silicon Photomultipliers. Available online: http://sensl.com/products/silicon-photomultipliers/ (accessed on 3 July 2021).
33. Magnan, P. Detection of visible photons in CCD and CMOS: A comparative view. *Nucl. Instrum. Meth. Phys. Res. A* **2003**, *504*, 199–212. [CrossRef]
34. Rowlands, J.A.; Yorkston, J. Flat Panel Detectors for Digital Radiography. In *Handbook of Medical Imaging Physics and Psychophysics*; Beutel, J., Kundel, H., Van Metter, R., Eds.; SPIE: Bellingham, WA, USA, 2000; Volume 1, pp. 223–328. ISBN 978-08-194-7772-9.
35. Cavouras, D.; Kandarakis, I.; Panayiotakis, G.S.; Bakas, A.; Triantis, D.; Nomicos, C.D. An experimental method to determine the effective efficiency of scintillator-photodetector combinations used in x-ray medical imaging systems. *Br. J. Radiol.* **1998**, *71*, 766–772. [CrossRef] [PubMed]
36. Advatech UK. LSO:Ce—Lutetium Oxyorthosilicate (Ce). Available online: https://www.advatech-uk.co.uk/lso_ce.html (accessed on 25 June 2021).
37. Advatech UK. BGO—Bismuth Germanate Scintillator Crystal. Available online: https://www.advatech-uk.co.uk/bgo.html (accessed on 25 June 2021).
38. Valais, I.; David, S.; Michail, C.; Nikolopoulos, D.; Vattis, D.; Sianoudis, I.; Cavouras, D.; Nomicos, C.; Kandarakis, I.; Pa-nayiotakis, G. Comparative study of luminescence properties of Lu_2SiO_5:Ce and $YAlO_3$:Ce single crystal scintillators for use in medical imaging. In Proceedings of the 5th European Symposium on Biomedical Engineering, Patras, Greece, 5–7 July 2006.
39. Roncali, E.; Stockhoff, M.; Cherry, S.R. An integrated model of scintillator-reflector properties for advanced simulations of optical transport. *Phys. Med. Biol.* **2017**, *62*, 4811–4830. [CrossRef]